Assessment of the physical vulnerability of buildings affected by slow-moving landslides

Qin Chen[1], Lixia Chen[2*], Lei Gui[1], Kunlong Yin[1], Dhruba Pikha Shrestha[3], Juan Du[4], Xuelian Cao[2]

[1]Engineering Faculty, China University of Geosciences, Wuhan, 430074, China

[2]Institute of Geophysics and Geomatics, China University of Geosciences, Wuhan, 430074, China

[3]Department of Earth Systems Analysis, Faculty of Geo-Information Science and Earth Observation (ITC), University of Twente, 7500 AE Enschede, the Netherlands

[4]Three Gorges Research Center for geo-hazard, Ministry of Education, China University of Geosciences, Wuhan, 430074, China

**Corresponding author:* Lixia Chen (lixiachen@cug.edu.cn)

Abstract: Physical vulnerability is a challenging and fundamental issue in landslide risk assessment. The previous studies mostly focus on generalized vulnerability assessment from landslides or other types of slope failures, such as debris flow and rock fall, while the long-term damages induced by slow-moving landslides are usually ignored. In this study, a method was proposed to construct physical vulnerability curves for masonry buildings by taking Manjiapo landslide as an example. Landslide force acting on the buildings' foundation is calculated by applying landslide residual thrust calculation method. Considering four rainfall scenarios, the buildings' physical responses from the thrust are simulated in terms of potential inclination by using the Timoshenko's deep beam theory. By assuming landslide safety factor as landslide intensity and inclination ratio as vulnerability, a physical vulnerability curve is fitted and the relative function is constructed by applying a Weibull distribution function. To investigate the effects of buildings' parameters that influence vulnerabilities, the length, width, height, foundation depth, and Young's modulus of the foundation are analysed. The validation results on the case building show that the physical vulnerability function can give a good result in accordance with the investigation in the field. The results demonstrate that the building length, width, and foundation depth are the three most critical factors that affect physical vulnerability value. Also, the result shows that the higher the ratio of length to width of the building, the more serious is the damage to the building. Similarly, the shallower the foundation depth, the more serious will be the damage. We hope that the established physical vulnerability curves can serve as tools for the quantitative risk assessment of slow-moving landslides.

Keywords: slow-moving landslides; physical vulnerability; building; vulnerability curves; risk

1 Introduction

Physical vulnerability is a fundamental and indispensable item in the risk definition presented by Varnes (1984). It can be defined as the degree of loss to a given element or set of elements within an area affected by a hazard (UNDRO, 1984). Physical vulnerability is measured on a continuous scale ranging from 0 (no loss) to 1 (total loss). For quantifying physical loss, such as the structural damage, the physical vulnerability of the elements at risk can be achieved by assessing the damage degree, resulting from the occurrence of a landslide of a given type and intensity (Van Westen et al., 2006).

Recently, physical vulnerability is still a challenge, and there has been a growing interest in quantifying risk due to natural hazards (Van Westen et al., 2006). To quickly and easily analyze the physical vulnerability, researchers have developed various types of tools or software such as HAZUS-MH (FEMA, 2003), RiskScape (King and Bell, 2005), ARMAGEDOM (Sedan et al., 2013), and CAPRA (https://ecapra.org/). HAZUS-MH (FEMA, 2003) is considered to be the initially introduced and the most popularly applied software. RiskScape is a national-scale multi-hazard impact model in New Zealand, and ARMAGEDOM is a tool for seismic risk assessment that has three different precision levels (regional territorial scale, district-scale, and the district-scale with more detailed hazard description and physical vulnerability estimation). The majority of the software is employed to analyze the physical vulnerability of earthquakes or multi-hazards, and very few can be utilized for landslide hazard assessment. To solve this problem, Papathoma–Köhle et al. (2015) developed an integrated toolbox designed for buildings subjected to landslides.

In the past decades, researchers have worked on landslide physical vulnerability assessments techniques, which can be grouped into four main approaches as follows: expert judgment (Sterlacchini et al., 2007; Winter et al., 2014; Godfrey et al., 2015; Guillard–Goncalves et al., 2016), statistical (Ciurean et al., 2013; Ciurean et al., 2017), mechanics-based (Luna et al., 2014; Liang and Xiong, 2019; Nicodemo et al., 2020), and integrated (Li et al., 2010; Uzielli et al., 2015b). The results of these approaches include matrices, indicators, and fragility, or physical vulnerability curves or functions. For example, by utilizing the procedures motivated by the seismic risk analysis, Negulescu and Foerster (2010) introduced a simplified methodology to evaluate the mechanical performances of buildings subjected to landslide hazards. Also, Totschnig et al. (2011) presented physical vulnerability curves for debris flow and torrent hazards. Wu et al. (2011) constructed physical vulnerability curves for landslides by considering the landslides' impact energy and impact impulse as the intensity indicators. By utilizing FLO-2D (a hydrologic and hydraulic modeling software of debris flow propagation), Luna et al. (2014) discussed the physical vulnerability functions of buildings at debris flow risk. Based on the physical vulnerability assessments proposed by Li et al. (2010), Uzielli et al. (2015b) modified the method by integrating the assessment of landslide intensity and buildings resilience. Papathoma–Köhle (2015) related hazard intensity (debris-flow depth) with the loss of buildings' damage to buildings' physical vulnerability curves. Soldato et al. (2017) studied the empirical physical vulnerability curves for buildings by considering the

debris-flow depth, the flow velocity, and the impact pressure. Mavrouli et al. (2017) quantified the masonry-buildings' damage induced by rockfalls by calculating the impact force of falling rocks on masonry buildings.

The slow-moving landslides are particular types of landslides with slow velocity based on the classification provided by Cruden and Varnes (1996). Slow-moving landslides on the pre-existing sliding surfaces can cause differential settlement or tilt on structures. People are not usually endangered but damage to buildings and infrastructures may be high (Douglas, 2007). Slow-moving landslides are observed worldwide in many countries, e.g., Italy (Cascini et al., 2008; Antronico et al., 2015; Uzielli et al., 2015a; Nicodemo et al., 2017; Borrelli et al., 2018; Ferlisi et al.,2019), Canada (Clifton et al., 1986; Brooker and Peck, 1993; Moore et al., 2006; Barlow, 2000), China (Chen et al., 2016; Zhang et al., 2018; Dong et al., 2018; Wang et al., 2018), USA (Esser, 2000), and Australia (Jworchan et al., 2008).

Fell et al. (2008) suggested the estimation of the physical vulnerability of elements at risk for various landslide types. The slow-moving landslides may cause partial damage to buildings due to local displacement. The assessment methods for the physical vulnerability of slow-moving landslides are still limited. The aforementioned approaches are not very suitable since slow-moving landslides have different intensity indicators and different types of damages as compared to that from debris flows, rockfalls, or fast-moving landslides.

The performance analysis of buildings during the landslide and the inventory of the observed damage is a feasible methodology (Faella and Nigro, 2003). To investigate the physical vulnerability of the buildings impacted by landslides, numerous studies have been conducted regarding the acquisition of landslide deformation displacement or finding the statistical relation between the damage degree of buildings and landslide intensity (Mansour et al., 2011; Abdulwahid and Pradhan, 2017; Nicodemo et al., 2017; Peduto et al., 2017; Chen et al., 2016; Peduto et al., 2018). For example, Mansour et al. (2011) investigated the relationship between the movement and the expected extent of damage to urban settlements. Based on the persistent scatterer interferometry, Lu et al. (2014) obtained the slow-moving landslides velocity for estimating buildings' economic risk with a total affected area of more than 800 km^2. Ferlisi et al. (2015) reported that combining the differential interferometry (DInSAR) data and the results of supplementary damage surveys on the slow-moving landslides allowed the preliminary generation of a (maximum velocity) cause-effect (damage) relation. Peduto et al. (2017) applied landslide deformation (cumulative surface displacement and differential settlement) as the input variables to construct the empirical fragility and physical vulnerability curves for buildings. By applying the horizontal strains and angular distortions to the numerical model, Infante et al. (2016) generated physical vulnerability for buildings. Nicodemo et al. (2020) employed the equivalent frame method to analyze the damage of a representative building in case of a slow-moving landslide by numerical modeling. However, a detailed study on the physical vulnerability of buildings using mechanical analysis is not yet available.

This study proposes a method for assessing the physical vulnerability from the perspective of mechanics and obtains its changes during the process of slow-moving landslides. We first calculate the thrust force of landslide acting on the buildings' foundation and then analyze the buildings' physical response. Multi-scenarios were applied to help in constructing the physical vulnerability curves. After the validation by utilizing an application on a typical building impacted by slow-moving landslides, a sensitivity analysis was conducted on the parameters of the building and its foundation.

2 Proposed method

2.1 Force acting on the building foundation during the landslide process

To quantitatively evaluate the building's physical vulnerability during the landslide process, it is essential to calculate the force acting on the building's foundation. In this study, landslide residual thrust force is calculated by employing the residual thrust method, which is extensively applied in China for slope stability analysis (Nie et al., 2004). A slide-mass is divided into different slices in this method and a force analysis is performed on each slice. In this way, it is possible to easily obtain the thrust of a landslide by utilizing the arbitrary shape of the sliding surface and under complex loads. The landslide residual force can be calculated by applying Eq. (1)–(6). In this method the groundwater seepage should be considered under rainy conditions, which can be performed using the SEEP/W code (GEOSTUDIO). The physical vulnerability curve is estimated using landslide safety factor to express the strenght of landslide. Landslides with smaller safety factors are more unstable, resulting in greater residual thrust on the building's foundation.

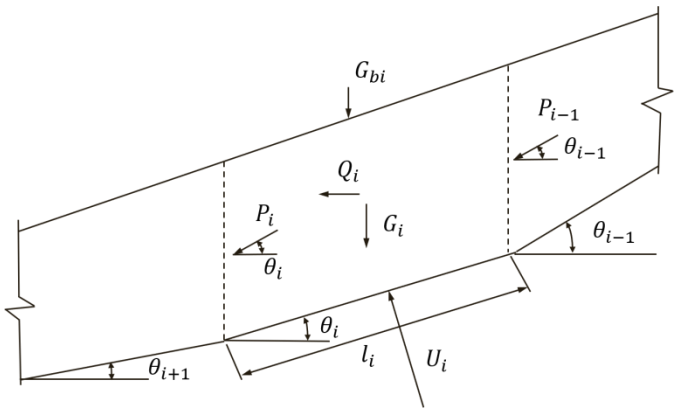

Fig. 1. Computing model of residual thrust method with a broken-line slip surface (Ministry of Housing and Urban–Rural Development of PRC, 2013).

The safety factor of landslide, F_s, is defined based on Chinese code of *Technical Code for Building Slope Engineering* (GB 50330-2013) as follows:

$$F_s = \frac{\sum_{i=1}^{n-1}\left(R_i \prod_{j=1}^{n-1} \psi_j\right)+R_n}{\sum_{i=1}^{n-1}\left(T_i \prod_{j=1}^{n-1} \psi_j\right)+T_n}, \quad (1)$$

For a single slice, the residual thrust force of the ith slice is given as follows:

$$P_i = P_{i-1} \times \psi_{i-1} + T_i - R_i/F_s, \quad (2)$$

$$F_i = P_i \times cos\theta_i, \quad (3)$$

$$R_i = [(G_i + G_{bi})sin\theta_i - Q_i sin\theta_i - U_i] \times tan\varphi_i + c_i l_i, \quad (4)$$

$$T_i = (G_i + G_{bi}) \times sin\theta_i + Q_i \times cos\theta_i, \quad (5)$$

$$\psi_{i-1} = cos(\theta_{i-1} - \theta_i) - sin(\theta_{i-1} - \theta_i)tan\varphi_i/F_s, \quad (6)$$

where R_i denotes the resistance force of ith slice (kN/m), T_i denotes the driving force of ith slice (kN/m), P_i denotes the residual thrust of ith slice (kN/m), ψ_i denotes the transmitting coefficient of ith slice, G_i denotes the weight of ith slice (kN/m), G_{bi} denotes the accessional vertical load of ith slice (kN/m), θ_i denotes the angle between the sliding surface and horizontal plane of the ith slice, l_i denotes the length of ith slice (m), c_i denotes the cohesion of ith slice (kPa), φ_i denotes the internal friction angle of ith slice, U_i denotes the pore water pressure of ith slice (kN/m), Q_i denotes the horizontal seismic force of ith slice, and F_i denotes the horizontal component of landslide thrust (shown in Fig. 2).

The transformation of landslide residual thrust force on buildings' foundation depends on the distribution of force. According to Chinese standard (China Railway Second Survey and Design Institute, 1983) and Dai (2002), landslide thrust distribution is approximately assumed to be triangular, rectangular, or parabola shapes, based on the type of sliding mass materials. Each type of thrust distribution corresponds to a distribution function (Table 1).

Table 1. Distribution functions of landslide thrust for various sliding mass materials of the landslide.

Soil types	**Distribution form** (referred to China Railway Second Survey and Design Institute (1983))	**Distribution functions** (Referred to Dai(2002))
Clay, Soil-rock, Rock	Rectangle or parallelogram	$q(z) = \frac{F}{d}$
Sand	Triangle	$q(z) = \frac{2F}{d^2}z$
Between clay and sand	Parabola shape	$q(z) = \frac{1.8F}{d^2}z + \frac{F}{10d}$

Note: F denotes the horizontal component of landslide residual thrust (P_i) in Eq. (3), and h denotes the vertical distance from the sliding surface to the ground surface (Fig. 2).

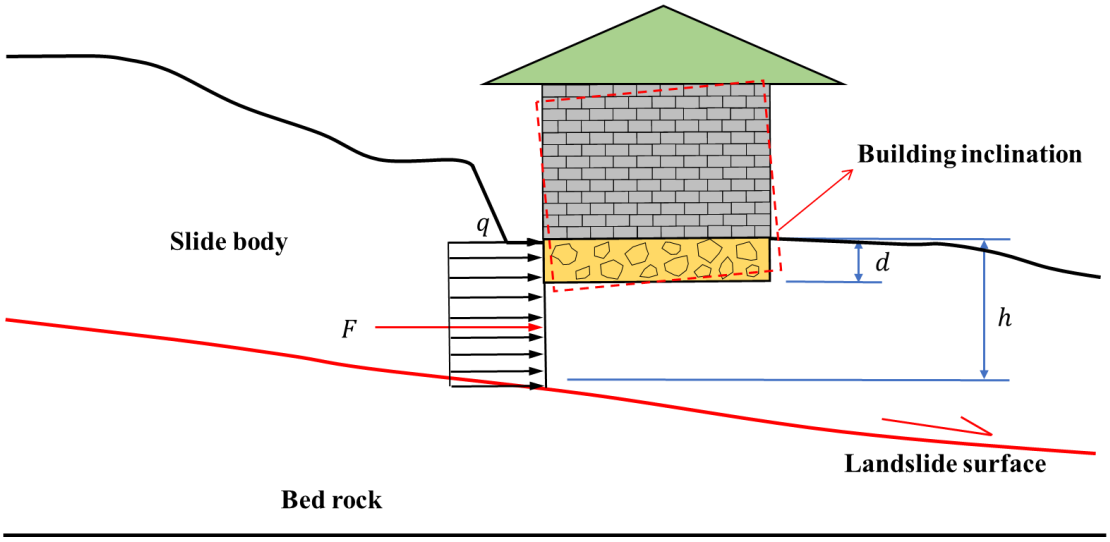

Fig. 2. A schematic diagram of landslide thrust action on a building.

2.2 Physical response of buildings

2.2.1 Inclination of buildings

The foundation of the masonry building affected by the landslide thrust can be simplified as a beam (Fig. 3). It has been observed that real structures are normally very complicated, but the simplification of the beam helps in illustrating several important features (Burland, 1974).

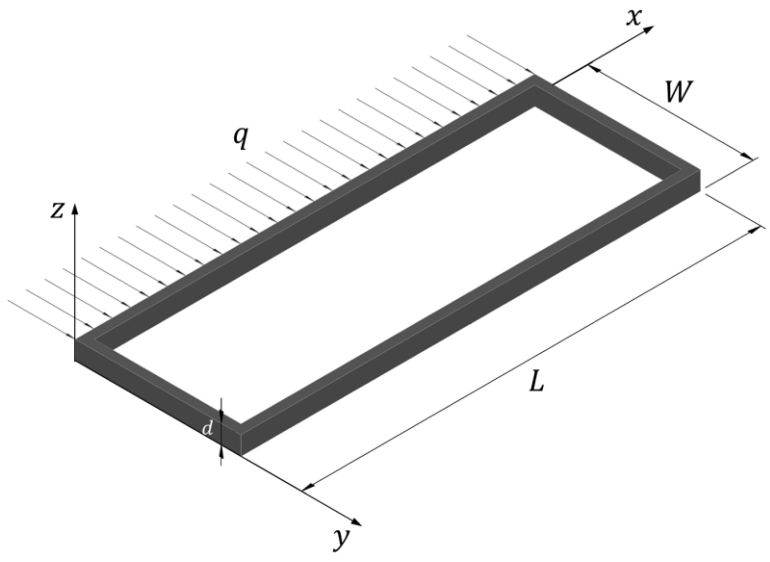

Fig. 3. The simple beam with its foundation affected by landslide thrust.

For illustrative purposes, we only consider the case of a beam with a uniform load. Timoshenko (1984) gave the function of deflection for the uniform loaded beam of unit thickness flexing in both shear and bending as follows:

$$y(x) = \frac{qx}{24EI}\left(\frac{x}{L}\right)\left(\frac{x^3}{L^3} - 2\frac{x^2}{L^3} + 1\right) + \frac{3qL^2}{4GA}\left(\frac{x}{L}\right)\left(1 - \frac{x}{L}\right), \quad (7)$$

where q denotes the distribution force on the foundation (kN/m), L denotes the length of the building, I denotes the moment of inertia defined by $I = \frac{dW^3}{12}$, in which d denotes the depth of the foundation, and W denotes the width of the building. Also, E and G denote Young's modulus and shear modulus of the foundation materials, respectively.

When $= \frac{L}{2}$, the equation for the total central deflection is the following:

$$y_m = \frac{5qL^4}{384EI} + \frac{3qL^2}{16GA}, \tag{8}$$

where the maximum deformation of the foundation is denoted by y_m.

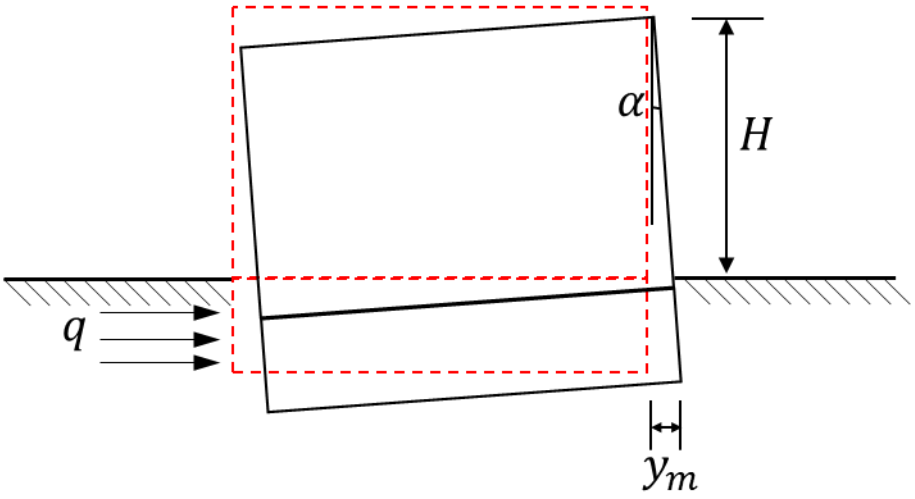

Fig 4. The inclination of the building

From *Technical Specification for Incline-rectifying of Buildings* (JGJ 270-2012), it is proposed that the incline angle of the building is the angle between the vertical plane of inclined building and the vertical plane of the original design building or the angle between the bottom plane of displacement foundation and the horizontal plane of foundation bottom of the original design. The angle α is the incline angle of the building shown in Fig 4. Furthermore, the inclination of the building is the tangent value of the incline angle.

Meanwhile, according to *Code of Deformation Measurement of Building and Structure* (JGJ 8-2007), we can calculate the inclination of the building which is the ratio of the horizontal difference between observation point on the top of the building and observation point on the bottom of the building to the vertical height of the building after tilted. The formula is as follows.

$$i = tan\alpha = \frac{y_m}{H} \tag{9}$$

Where,

i --- the inclination of the building

α --- the incline angle of the building

y_m --- the horizontal difference between the top and bottom of the building

H --- the vertical height of tilted building calculated from the outdoor ground

It is worth pointing out that the building in our study case is regarded as a rigid building. So, the maximum horizontal displacement of the foundation by using the simple beam mechanical model will be approximately the horizontal difference of the observation point at the top of the building relative to the observation point at the bottom.

The following is the equation for the inclination of the building:

$$i = tan\alpha = \frac{y_m}{H} = \frac{1}{H}\left(\frac{5qL^4}{384EI} + \frac{3qL^2}{16GA}\right), \quad (10)$$

where i denotes the inclination of the building, which is the ratio of the maximum deformation y_m and the vertical height of tilted building calculated from the outdoor ground H.

2.2.2 Damage degree definition

In this study, the ratio of the building's inclination to the threshold value is represented as the damage degree. The damage degree is regarded as the output of physical vulnerability (Tarbotton et al.,2015, Kang et al.,2016). The degree of the building damage can be evaluated by utilizing some parameters, such as cracks in walls, inclination , the ratio of maintenance cost and the original value of building (Alexander, 1986; Chiocchio et al., 1997; Cooper, 2008). Finno et al. (2005) reported that when highly stiff buildings are very inclined due to ground deformation, the wall cracking phenomenon is not obvious. On the contrary, if the stiffness of the building is lower, the cracking on the wall becomes serious. This research shows that using only cracks as an indicator is not suitable for vulnerability assessment. Other indicators, such as inclination, should also be taken into consideration. Therefore, the width of the cracks is not the only indicator for building damage assesment but we should also take into account if the building has inclined. Therefore, the inclination has been chosen to represent the deformation of buildings (Huang, 2015).

Moreover, the inclination of the building is easy to measure. The standard for dangerous building appraisal (JGJ125-2016 China) provides the threshold value of the inclination of single- or multi-story buildings (Table 2). Buildings with inclination exceeding the threshold value are considered to be dangerous and uninhabitable.

Table 2. The threshold value of building inclination (Ministry of Housing and Urban–Rural Development of PRC, 2016).

Height（m）	$H_g \leq 24$	$24 < H_g \leq 60$	$60 < H_g \leq 100$
Threshold value i_m	1%	0.7%	0.5%

Here, H_g denotes the building height which is calculated from the outdoor ground.

By comparing the inclination of the building with the threshold value, the vulnerability (V) can be calculated as follows:

$$V = \begin{cases} \frac{i}{i_m} = \frac{1}{Hi_m}\left(\frac{5qL^4}{384EI} + \frac{3qL^2}{16GA}\right) & (i < i_m) \\ 1.0 & (i \geq i_m) \end{cases}. \quad (11)$$

The vulnerability (V) ranges from 0 to 1.0, value close to 1.0 indicates serious damage. Equation (11) demonstrates that the building's inclination depends on the following three parameters: size, material, and foundation depth. To ascertain the

parameter with the highest significant impact on the degree of building damage, we can conduct a sensitivity analysis on these parameters by employing the principle of controlling variables.

2.3 Physical vulnerability function for masonry buildings

2.3.1 General functions

In this study, we obtained the physical vulnerability curve by relating building vulnerability with landslide safety factor (F_S). It is important to note that F_S is calculated for only the area where the building under study is located, but not for the whole landslide area. Landslide intensity is directly proportional to its stability situation. A higher intensity corresponds to a higher thrust force on the building foundation and lower landslide safety factor. Thus, we utilize the reciprocal value of F_S to be the landslide intensity in this study.

The relationship between building vulnerability and the landslide intensity was fitted by employing Weibull (1951) function that produces an S-shaped curve. This type of distribution curve has been proved to be the best for physical vulnerability analysis by Dario Peduto et (2017), Kang et (2016), Papathoma–Köhle et al. (2015), and Negulescu et (2010). Based on these findings, a modified Weibull function for calculating physical vulnerability is defined as follows:

$$V = 1 - e^{-a\left(\frac{1}{Fs}\right)^b}, \tag{12}$$

where V denotes physical vulnerability which is calculated by employing Eq. (11) ; Fs is calculated by employing Eq. (1) ; a and b are constants, which need to be determined.

2.3.2 Determination of constants by applying multiple scenarios

To determine the constants a and b in Eq. (12), we first obtain two or more scenarios, which can reflect the landslide safety factor and the building vulnerability. Using several triggering scenarios, such as rainfall, earthquake, and reservoir water level fluctuation, we can obtain several safety factors, the corresponding landslide force on building foundation, and the building vulnerability. Then, we apply the least-square method to obtain the constants based on the presupposed function in Eq. (12).

In this study, rainfall is the key triggering factor for the landslide. Thus, we obtain rainfall scenarios by analyzing the precipitation using different return periods. Pearson type (PT) III distribution model (Lei et al., 2018; Radwan et al., 2019) is applied because it is useful in rainfall-induced landslides; its probability density function is defined as follows:

$$f(x) = \frac{\beta^\alpha}{\Gamma(\alpha)}(x - a_0)^{\alpha-1}e^{-\beta(x-a_0)}, \tag{13}$$

where parameters α, β, a_0, can be given by the following three statistical parameters after conversion: $(\dot{x}, C_v, C_s)$. Thus, we have

$$\alpha = \frac{4}{C_s^2}$$
$$\beta = \frac{2}{\acute{x} C_v C_s} \quad , \tag{14}$$
$$a_0 = \acute{x}\left(1 - \frac{C_v}{C_s}\right)$$

where $\acute{x}$ denotes the average value, C_v denotes the coefficient of variation, and C_s denotes the coefficient of skewness.

From Eq. (14), the PT III distribution model has three undetermined parameters: $\acute{x}, C_v, C_s$. The principle of maximum entropy, the methods of moments, and maximum likelihood estimation are employed to estimate the parameters for the PT III distribution (Singh and Singh, 1988). We plot the physical vulnerability curve after obtaining the values of these three parameters determined by different rainfall scenarios with varying return periods.

3 Application of the proposed method

3.1 Geological settings and deformation of landslide

The Manjiapo landslide (110°10′0.32″E, 29°25′3.69″N), located in Sangzhi County, Zhangjiajie, China was selected as the case study (Fig. 5). The area is mountainous and hilly with elevation ranging from 154 m to 1890 m a.s.l. The climate is humid subtropical, and the estimated average annual rainfall is about 1400 mm.

The landslide covers an area of about 6.6×10^4 m^2 with an average thickness of 6.9 m and an estimated volume of 45.5×10^4 m^3. It demonstrates strip shape in a plan with a longitudinal dimension of about 560 m and the average width of approximately 176 m along the northwest (NW)–southeast (SE) direction. The elevation of the main crack is about 370 m a.s.l. The toe of the landslide is located at 272 m elevation along the stream.

The topography demonstrates a multi-step shape, the height of which ranges from 1 to 3 m. The middle and upper parts of the landslide are relatively gentle with a slope gradient of about 8°， while the lower part is steeper (12° slope). The sliding direction of the landslide includes two parts: the upper part orients at 335°, and the lower part at 313°.

The main materials of the landslide comprise loose debris from silty clay and siltstone, in which the latter only distributes in the middle and upper sections of the landslide (Fig. 6). The bedrock is argillaceous siltstone with a slope angle of approximately 10°. The shear-strength parameters of the slip soil of the landslide, shown in Table 3, are obtained from the detailed landslide report 2017 of the Hunan Institute of Xiangxi Geological Engineering Survey. The shear-strength parameters are based on 6 groups of undisturbed soil samples and their laboratory tests.

Table 3. Shear-strength parameters of Manjiapo landslide slip soils (data source: Hunan Institute of Xiangxi Geological Engineering Survey, China).

	Dry condition		Saturated condition	
	c/kpa	$\varphi/(°)$	c/kpa	$\varphi/(°)$
Average	11.98	9.09	5.85	6.84
Variance	1.56	2.25	0.79	0.64

Manjiapo landslide has a history of 10-year displacement. According to the residents, the landslide occurred in August 2008, which resulted in a few ground fissures. Due to heavy rain during 28th to 30th June in 2016 induced severe displacement of the landslide. Field investigation carried out in July 2017 revealed that the displacement mainly occurred in the middle and upper parts of the landslide (Figs.5c and 7a,b). Numerous tension cracks in the upper part had a visible depth of 2–5 cm, with a length of 1 600 to 6 600 cm and a width of about 15 cm . In the middle part of the landslide, staggered extrusion deformation can be observed locally apart from numerous tension cracks.

Moreover, the surface deformation caused the rise of groundwater in the silty clay layer. As a result, the shear strength of the soil mass decreased and the sliding zone was formed. It was revealed by boreholes dug during fieldwork in 2017. On the lower part of the landslide, cracks and some uplift deformation were observed on the roads (Fig. 7c).

Rainfall appeared to be the most important triggering factor of the slow-moving Manjiapo landslide. The cracks and the macroscopic deformation on the landslide were monitored since 2016. Analysis of the monitoring data shows that only heavy rainfall could reactivate the landslide. Analysis of the borehole data shows that the groundwater table is stable in the dry season. The landslide did not show any displacement in the absence of extreme rainfall. For example, the cracks on the landslide did not expand, and there were only a few new cracks.

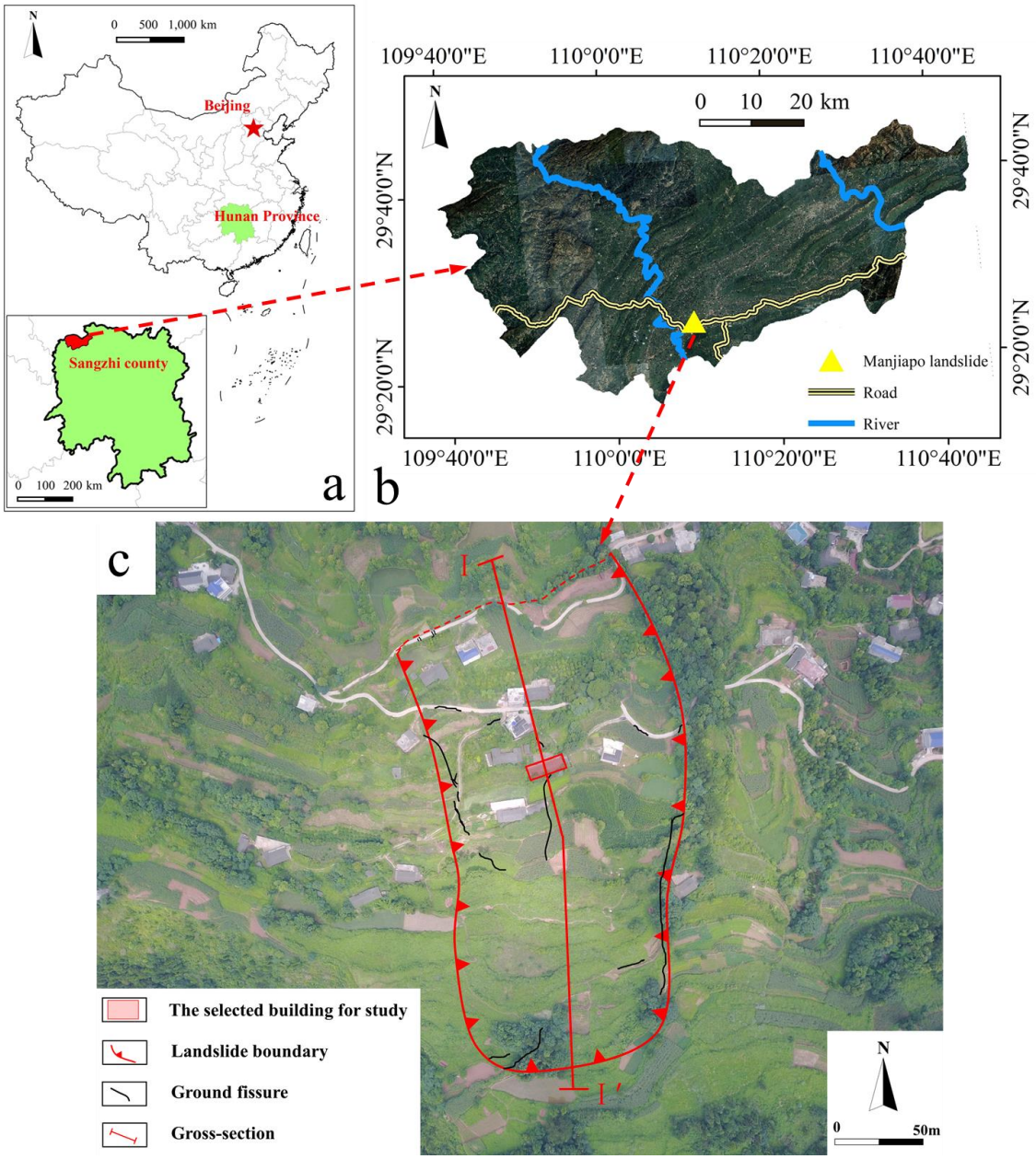

Fig. 5. Location of the Manjiapo landslide, a) map of China download from http://www.geodata.cn, b) a Google Earth image fragment showing the location of the landslide, and c) an Unmanned Air Vehicle (UAV) image showing the landslide boundary and the location of a cross-section I-I′ (UAV image obtained during field investigation).

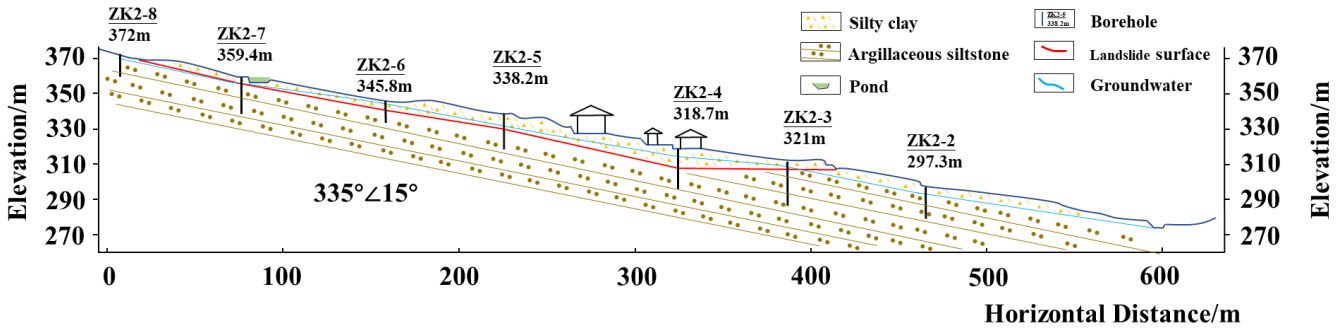

Fig. 6. Geological profile (1:1 000) of section *I-I′* of the Manjiapo landslide. The location of the cross-section is shown in Fig. 5c.

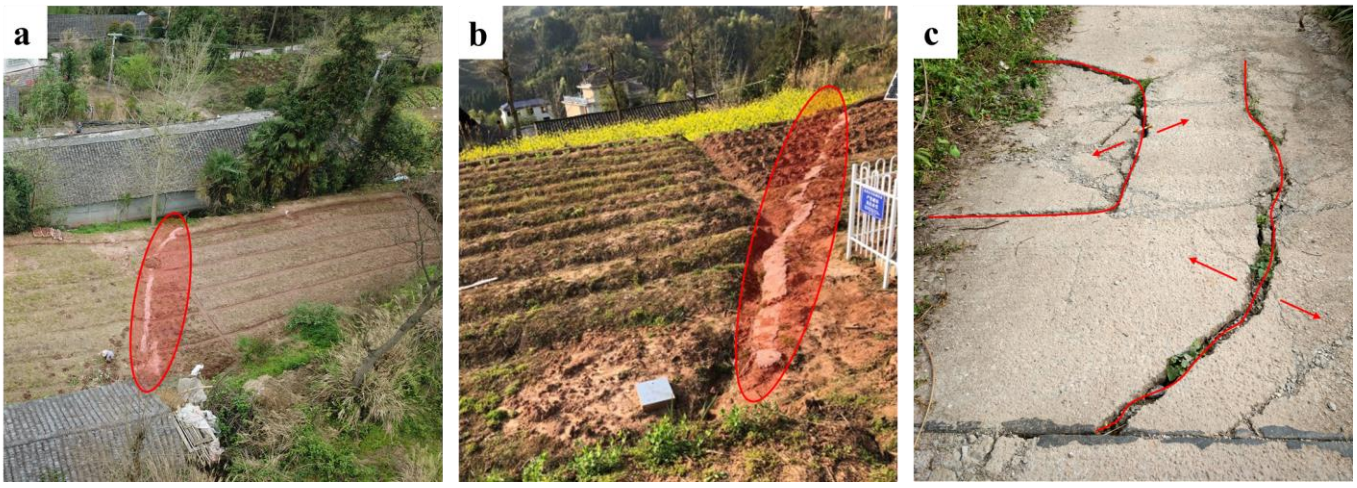

Fig. 7. Cracks on the Manjiapo landslide: (a) the middle part, (b) the upper part, and (c) the lower part.

3.2 Damaged buildings on the landslide

Field investigation, carried out in July 2017, shows that 15 houses were affected by the landslide, of which 5 were constructed using brick-wood and 10 brick-concrete (Fig. 8). The buildings located in the middle part of the landslide were the most severely damaged. Due to landslide deformation, the walls of these buildings were cracked and inclined. We selected a damaged building for a detail study. Severe cracks appeared on the walls, and finally, the building was abandoned.

The selected building for study is a story masonry building with a length of 25 m and a width of 9 m. The building has six rooms, and each room was damaged as a result of continuous rain from June 28th to 30th in 2016. Large-scale ground collapse occurred in rooms C， D, and E (Fig. 9). Meanwhile, the walls of these rooms developed numerous diagonal cracks with width varying from 2 to 8 cm. The walls were heavily tilted, with inclination varying from 0.7% to 1.0% (Fig. 10a,b,c).

Table 4. Parameters of the building on Manjiapo landslide

For building				For foundation			Soil depth where the building located (m)
Length L (m)	Width W (m)	Height H (m)	Depth d (m)	Young's modulus E (MPa)	Shear modulus G (MPa)	E/G	
25	9	2.8	1	2250	865	2.6	5

Remark: The elastic modulus value is called the code for the design of masonry building (GB50003-2011). Thus, an isotropic elastic material is defined as follows: $E/G = 2(1+\nu)$, where ν denotes the Poisson's ratio for $\nu = 0.3$, and $E/G = 2.6$ (Burland, 1977). H denotes the vertical height of tilted building calculated from the outdoor ground.

Fig. 8. A typical example of a damaged building in the landslide area (Unmanned Air Vehicle image obtained during field investigation).

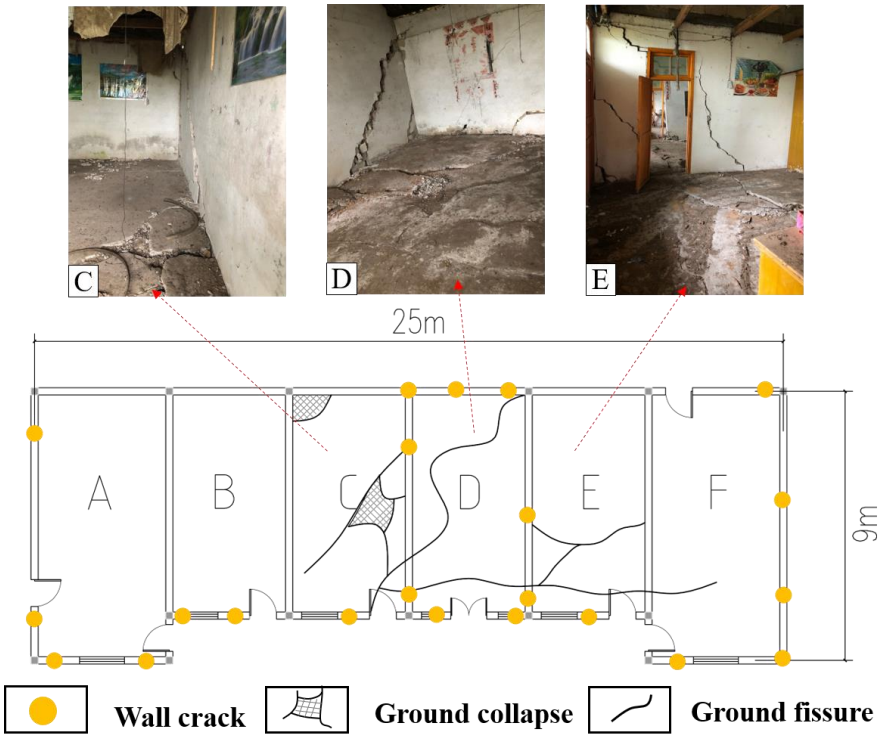

285 **Fig. 9. Floor plan of the case study building.**

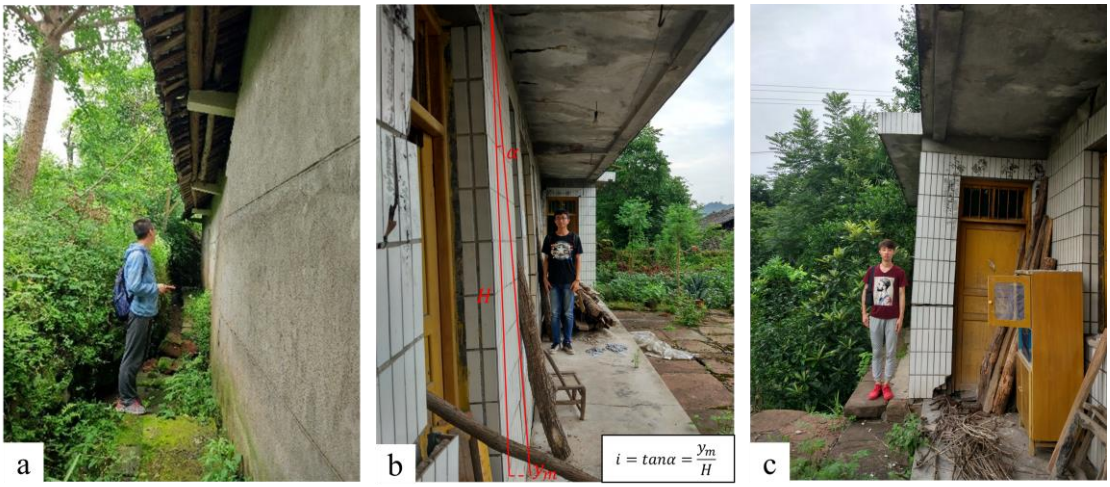

Fig. 10. The integral decline state of the case study building:(a) the back wall of the building with inclination of 1.0%,(b) the front wall of the building with inclination of 0.8%,(c) the front wall of room A (shown in fig 9)with inclination 0f 0.7%

290 *3.3 Rainfall data analysis*

Landslides are induced by extreme or short-term sustained intense precipitation (Chen et al., 2014； Qiong et al., 2018； Huang et al., 2014). Furthermore, 3-day rainfall proved to be the most relevant parameter of landslide occurrences in the study area (Lin et al., 2018). Precipitation data of Sangzhi County for the period 1995 to 2016 were collected from the sitehttp://www.cma.gov.cn/. The data was analyzed for extreme rainfall and scenario determination (Fig. 11).

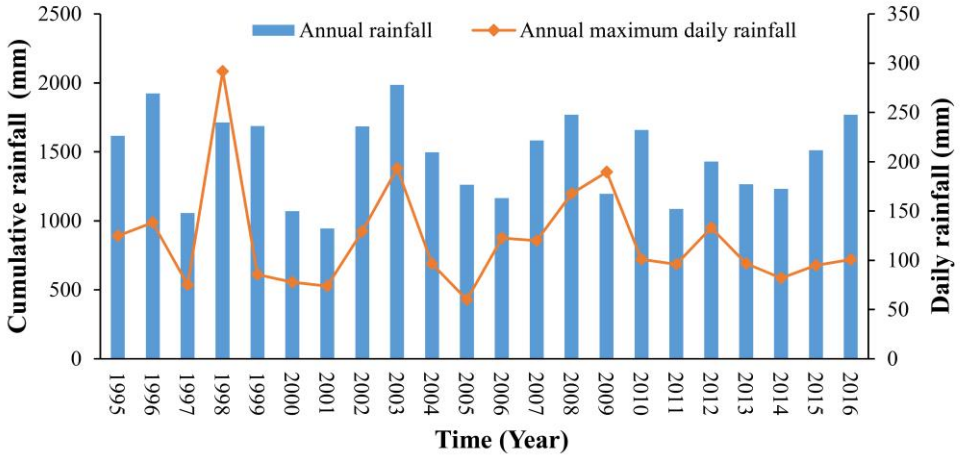

295

Fig. 11. Annual and maximum daily rainfall in the study area during the period of 1995–2016.

4 Results

4.1 Extreme rainfall scenarios and landslide residual thrust calculation

The extreme rainfall distribution curve is depicted in Fig. 12 that is constructed by employing PT III distribution model and

300 the rainfall data collected for the period 1995-2016. Using this curve, we can obtain the amount of 3-day cumulative precipitation corresponding to each return period.

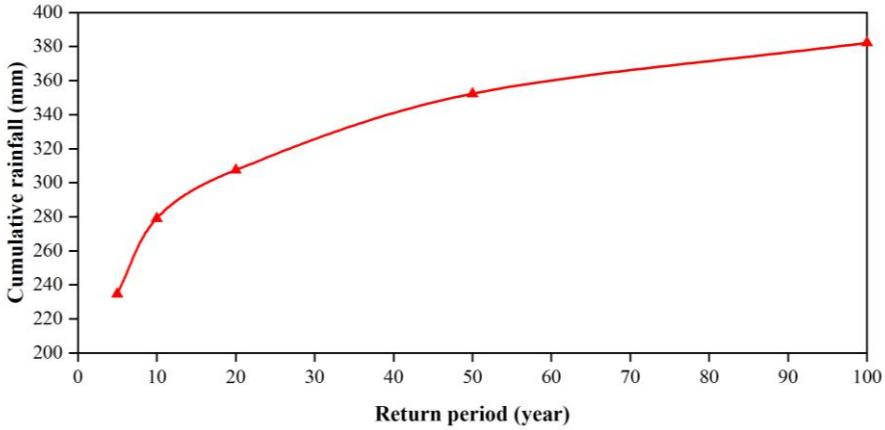

Fig. 12. The extreme rainfall distribution curve.

Groundwater levels based on four scenarios with different magnitudes of rainfall were selected: (a) dry condition, no rain; (b) rainfall with a return period of 5 years (3-day precipitation 235 mm from Fig. 11); (c) rainfall with a return period of 10 years (3-day precipitation 279 mm from Fig. 11); (d) rainfall with a return period of 50 years (3-day precipitation 352 mm from Fig. 11). For scenarios b, c, and d, rainfall data was utilized as the boundary condition to simulate the groundwater level of the landslide. Note that all the scenarios are assumed without the influence of an earthquake.

The SEEP/W code (GEOSTUDIO) was applied to analyze the groundwater seepage of Manjiapo landslide to obtain the amount of 3-day cumulative precipitation corresponding to each return period by using PT (Pearson type) Ⅲ distribution model(Fig. 12). The average amount of 3-day cumulative precipitation is input to the software in turn, and the groundwater under the rainfall scenarios is simulated.

The saturated volumetric water content is 0.4 by cutting the ring method. The saturated permeability coefficient is obtained by back analysis. We choose the saturated volumetric water content and the permeability coefficient by the variable-controlling approach. Three groups of input values are: 0.4, 0.1; 0.4, 0.2; 0.4, 0.3. Then, the groundwater is simulated and validated for the rainfall event in March 2018. The root mean square error (RMSE) is utilized to check the accuracy. Lower RMSE means smaller error and better prediction. The results of the RMSE are shown in the following table. The saturated volumetric water content is 0.4 and the most suitable permeability coefficient is 0.3 m/d.

Table 5. Permeability coefficient back analysis of the rainfall event in March 2018, by comparing the root mean square errors (RMSE) of three hydrological gauges (installed by the authors in December 2017, see Fig.5) on the Manjiapo landslide

The permeability coefficient (m/d)	0.1	0.2	0.3
RMSE (STK-1)	2.280	2.222	2.154
RMSE (STK-2)	0.860	0.677	0.615
RMSE (STK-3)	2.540	2.491	2.405

Note: the saturated volumetric water content by Lab test is 0.4.

The results of the residual thrust and the corresponding safety factor are presented in Table 6. These values were obtained by the landslide residual force calculation method (section 2.1) for the geological profile (Fig. 6). In the dry season (scenario

a), the landslide performs residual thrust of 142 kN/m and safety factor for the area where the case study building is located of 0.853, while the these values can change significantly in rainy season (scenario b, c and d). For an example, the residual thrust can be increased by at least 15 times and the safety factor can be reduced by nearly half in the rainy season with a 50-year rainfall. This indicates an important influence of rainfall on landslide stability and the building's safety.

Table 6. Landslide residual thrust, pushing force on the building's foundation, and vulnerability of the building based on four scenarios ((a) dry condition ; (b) rainfall with a return period of 5 years (3-day precipitation 235 mm/d); (c) rainfall with a return period of 10 years (3-day precipitation 279 mm/d) ; (d) rainfall with a return period of 50 years (3-day precipitation 352 mm/d)).

Scenarios	F_{sb}	F_s	F(kN/m)	q（kN/m）	i（%）	V
a	0.853	1.457	142	28	0.053	0.053
b	0.529	0.819	1756	351	0.656	0.656
c	0.481	0.778	2040	408	0.762	0.762
d	0.428	0.632	2638	528	0.985	0.985

Here, F_{sb} denotes the factor of safety for the area where the building is located.

4.2 Results of scenario-based vulnerability curve of the building

As described earlier in section 3.1 and demonstrated in the geological profile (Fig. 6), the sliding mass material is silty clay and bedrocks. Therefore, the thrust distribution form can be considered as rectangular based on Table 1. By applying the results of the horizontal component of landslide residual thrust (using the method in section 2.1) and the soil depth where the building is located (Table 3), the pushing force on the foundation was calculated by the corresponding thrust distribution function.

Table 6 illustrates the results of pushing force on the foundation, inclination, and the building vulnerability based on different scenarios. The result indicates that the building's vulnerability is very low (V = 0.053) in the dry season, with a pushing force of 28 kN/m on the building's foundation. However, in rainy seasons, the building can experience severe damage with the vulnerability of 0.798 (10-year rainfall) or even 0.985 (50-year rainfall).

Using the four sets of scenario data (Table 6), we constructed the physical vulnerability function and the constants in Eq. 12 were determined by employing the Weibull function.

Based on the Chinese standard of *Specification of Risk Assessment for Geological Hazard* (DZ/T 0286-2015), there are three stability states of landslide according to the range the safety factor (*Fs*) of landslide. Please see more details in the following table 7.

Table 7. The range of safety factor (F_s) of landslide and its state (referred to Ministry of Land and Resources of the PRC, 2015)

The safety factor F_s	$F_s \leqslant 1.00$	$1.00 < F_s \leqslant F_{st}$	$F_s > F_{st}$
Stability state of landslide	unstable	Less stable	stable
Description	(1) Many newly expanded cracks on the ground and new deformation on buildings and vegetation. (2) Obvious scratch	(1) Local deformation on the ground. (2) No obvious deformation on the main scarp. (3) No obvious expansion of	(1) No sustained deformation on the ground. (2) No crack expansion on the landslide. And no new deformation on buildings

	and displacement on the main scarp. (3) Cracks on the crown of landslide.	the cracks on the buildings. (4) Small cracks on the crown of landslide.	and vegetation on the landslide. (3) No scratch and obvious displacement on the main scarp.

Note: F_{st} denotes the design safety factor.

The value of F_{st} is defined based on the slope safety level and slope type. Meanwhile the slope safety level is defined based on the potential economic loss and element at risk. According to the field investigation, there are 116 residents in the affected area of the Manjiapo landslide, and the road passes through the middle part of the landslide. In case of geologic hazard, it will threaten the lives and property of 116 residents and damage more than 67,000 square meters of the land. At the same time, the road will be damaged, threatening the safety of the pedestrians and passing vehicles. The potential economic loss will be more than CNY 5 million. Based on the table 9 , the safety level of the Manjiapo landslide is judged to be second level.

Table 8. The value of the design safety factor (referred to Ministry of Housing and Urban–Rural Development of PRC, 2013)

the slope safety level		First level	Second level	Third Level
Permanent slope	General condition	1.35	1.30	1.25
	Earthquake condition	1.15	1.10	1.05
Temporary slope		1.25	1.20	1.15

Table 9.The slope safety level (referred to General Administration of Quality Supervision, Inspection and Quarantine of the PRC,2016)

the slope safety level		First level	Second level	Third Level
potential economic loss (CNY)		≥ 50 million	5 million to 50 million	< 5million
Element at risk	population	≥ 500	100 to 500	< 100
	Infrastructure	Very important	Important	less important

Note: If one of the conditions is met, it will be judged to be the corresponding slope safety level.

So, when the safety factory of the Manjiapo Landslide is greater than 1.30, the landslide is stable and the landslide intensity is very low. In addition, the resistance ability of the building can prevent the building from being destroyed by the low intensity of the landslide (Du, 2013). In summary, the physical vulnerability of the building on Manjiapo landslide is very low when the safety factory is greater than 1.30. It provides that the physical vulnerability of the building on Manjiapo landslide is 0 when the reciprocal value of the safety factor is 0.5. The physical vulnerability of the case study building on Manjiapo landslide is demonstrated in Fig. 13.

We can observe that the physical vulnerability is very low when the landslide is stable with a safety factor greater than 1.0. When the safety factor is lower than 1.0, the physical vulnerability rapidly increases. Vulnerability approximates 1.0 when the reciprocal value of the safety factor is 2.5. By utilizing this curve, we can obtain the possible physical vulnerability of the building if the safety factor of the landslide is known. Therefore, we need to demonstrate that the safety factor is for the local area where the case study building is located, but not for the whole landslide.

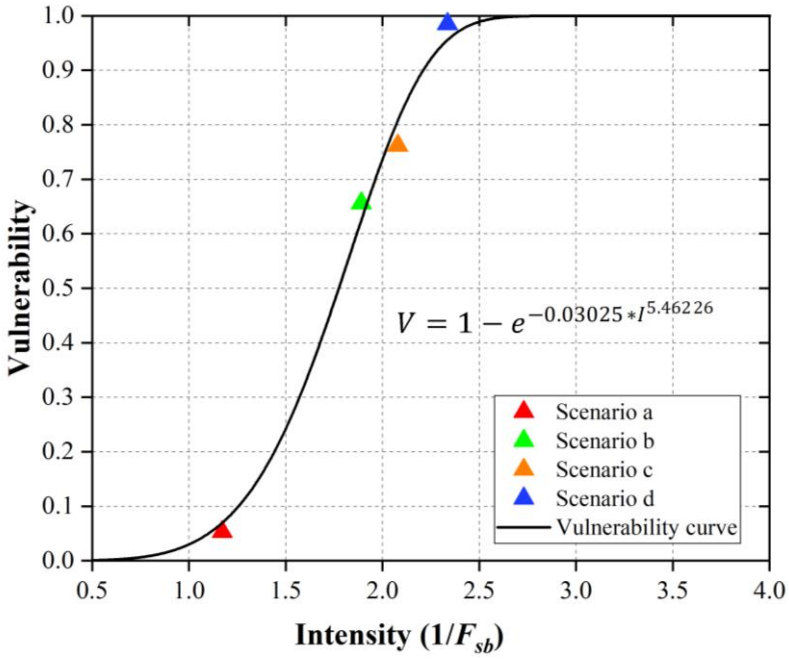

Fig. 13. The physical vulnerability curve for masonry buildings impacted by the slow-moving landslides.

4.3 Influence of building characteristics on vulnerability and the sensitivity analysis

To obtain the influence of building characteristics on vulnerability, we conducted sensitivity analysis. We know that numerous parameters of the building were included in the building inclination and vulnerability calculation e.g. length, width, depth of foundation, and E/G ratio . We conducted sensitivity analysis by changing the values of each parameter in step while keeping others constant and estimated the possible physical vulnerabilities of the building. The results are shown in Fig. 14.

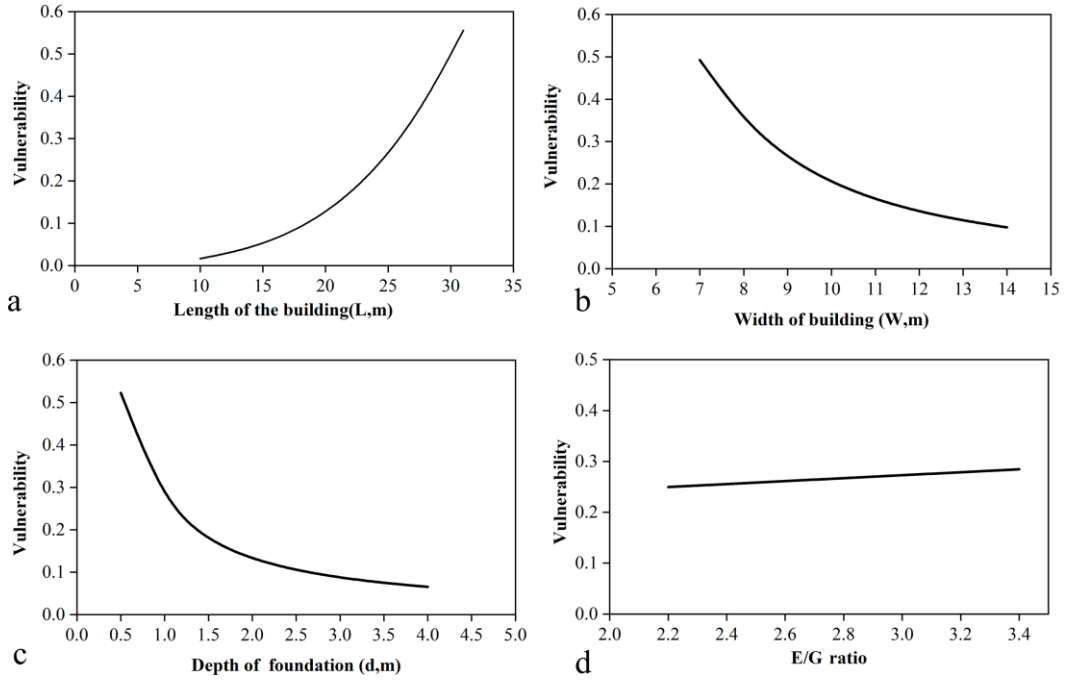

Fig. 14. Vulnerability curves for different building parameters: a) length, b) width, c) depth of foundation, and d) E/G ratio.

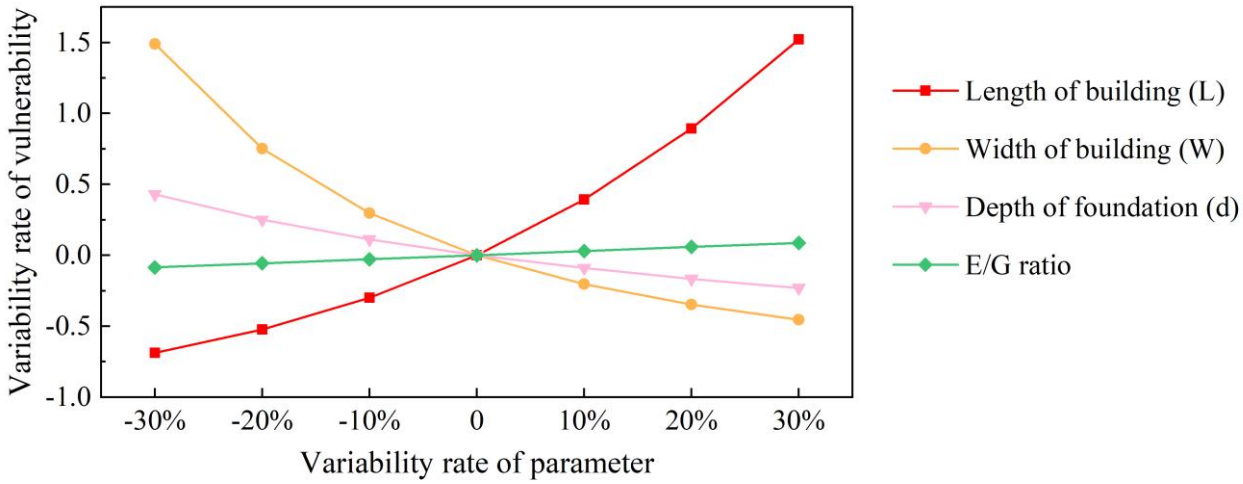

Fig. 15. The sensitivity analysis of building parameters for physical vulnerability.

As demonstrated in Fig. 14, we observe that the physical vulnerability is directly proportional to the building length, E/G ratio and is inversely proportional to the other parameters: building width, and foundation depth. It also shows that the higher the ratio of building length and width, the more vulnerable to damage the building is. Besides, buildings with deeper foundation and higher E/G ratio have higer resistance.

The results of the sensitivity analysis of the building parameters are demonstrated in Fig. 15. The red line that represents length has the steepest slope among all the lines, indicating that the length of the building has the most significant influence on the physical vulnerability of building. We can simultaneously obtain the second major factor that is the width of the building, while the third one is the foundation depth.

We tested four types of buildings with different lengths: 15 m, 20 m, 25 m, and 30 m (Fig. 16(a)). When F_{sb} is greater than 1.0, the building physical vulnerability with any length is very low, that is, almost no damage. In addition, the building demonstrated a different performance when F_{sb} is less than 1.0. The building physical vulnerability with length 15 m was slightly increased when the landslide stability was getting worse. However, the building physical vulnerability with length 30 m rapidly increased when F_{sb} was less than 1.0. This indicates that the buildings on the location where the target building stands have a limit length of 30 m. When the length of the building was greater than 30 m, the building faced severe damage if F_{sb} was less than 1.0.

To further test the detailed influences of the building parameters, we select the top two parameters based on the above results of sensitivity analysis: building length and width. Two sets of physical vulnerability curves are depicted in Fig. 16, and the corresponding functions of building physical vulnerability at the three scenarios are presented in Table 10.

a

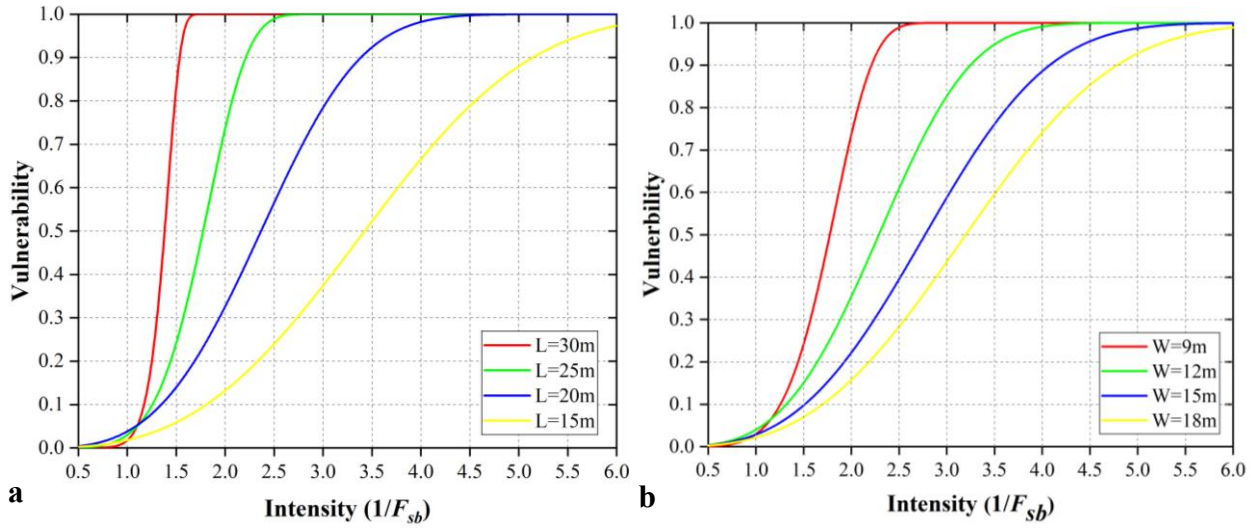

Fig. 16. Physical vulnerability curves of buildings with different parameters: (a) length and (b) width.

Physical vulnerability curves of buildings with various building width are depicted in Fig. 16(b), while the physical vulnerability curves of buildings with various lengths are depicted in Fig. 16(a). The difference in the physical vulnerability of the buildings with different building width is not significant when the F_{sb} is greater than 1.0. Meanwhile, the building with building width 9.0 is susceptible to the changes of F_{sb}. A rapid increase of building damage with such building width occurs when the F_{sb} is less than 1.0. When the building width is close to the building length, the vulnerability of the building is low under the same value of F_{sb}.

Table 10. Physical vulnerability functions of buildings with different lengths and width based on various scenarios.

Parameters		Scenarios	F_{sb}	F (kN/m)	i (%)	V	vulnerability function
Length (L/m)	15	a	0.853	142	0.010	0.010	$V = 1 - e^{-0.01827*(1/Fs)^{2.9535}}$
		b	0.529	1756	0.128	0.128	
		c	0.481	2040	0.149	0.149	
		d	0.428	2638	0.193	0.193	
	20	a	0.853	142	0.025	0.025	$V = 1 - e^{-0.03869*(1/Fs)^{3.34957}}$
		b	0.529	1756	0.312	0.312	
		c	0.481	2040	0.362	0.362	
		d	0.428	2638	0.469	0.469	
	25	a	0.853	142	0.053	0.053	$V = 1 - e^{-0.03025*(1/Fs)^{5.46226}}$
		b	0.529	1756	0.656	0.656	
		c	0.481	2040	0.762	0.762	
		d	0.428	2638	0.985	0.985	
	30	a	0.853	142	0.101	0.101	$V = 1 - e^{-0.01735*I(1/Fs)^{11.41247}}$
		b	0.529	1756	1.239	1.000	
		c	0.481	2040	1.440	1.000	
		d	0.428	2638	1.862	1.000	
Width (W/m)	9	a	0.853	142	0.053	0.053	$V = 1 - e^{-0.03025*(1/Fs)^{5.46226}}$
		b	0.529	1756	0.656	0.656	
		c	0.481	2040	0.762	0.762	
		d	0.428	2638	0.985	0.985	
	12	a	0.853	142	0.027	0.027	$V = 1 - e^{-0.04074*(1/Fs)^{3.42469}}$
		b	0.529	1756	0.338	0.338	
		c	0.481	2040	0.393	0.393	
		d	0.428	2638	0.508	0.508	
	15	a	0.853	142	0.017	0.017	$V = 1 - e^{-0.029*(1/Fs)^{3.11232}}$
		b	0.529	1756	0.214	0.214	

	c	0.481	2040	0.249	0.249	
	d	0.428	2638	0.322	0.322	
18	a	0.853	142	0.012	0.012	$V = 1 - e^{-0.02169*(1/Fs)^{2.97989}}$
	b	0.529	1756	0.153	0.153	
	c	0.481	2040	0.177	0.177	
	d	0.428	2638	0.229	0.229	

5 Discussion

We developed a scenario-based mechanical method for analyzing the physical vulnerability of buildings on slow-moving landslides. The method enabled us to analyze the physical vulnerability from a mechanical view on soil-structure interaction, which can help us to better understand the building damage on the slow-moving landslides and is useful for physical vulnerability assessment of masonry buildings loacated on slow-moving landslides. By inputing the geometry parameter (length and width of the buliding) and the safety factor of the area where buildings located, the potential vulnereability can be obtained by using the vulnerability functions we provided in this study.

The results of the application correspond to the fact from the field investigation. As described in section 3.2, the building damage occurred due to rainfall from June 28th to 30th, 2016. the calculated physical vulnerability is observed to be 0.762 (Table 5), which is close to the real damage measured in the field varied from 0.7 to 1.0 (Fig. 10a,b,and c). Herein, the influence of building parameters (length, width, height, foundation depth, etc.) on physical vulnerability corresponds to other previously conducted studies (Li et al., 2010; Du et al., 2013; Corominas et al., 2014). This is consistent with the study conducted by Corominas et al. (2014) that the typology of buildings is a key factor in the quantification of physical vulnerability.

The vulnerability funcitons from this study is suitable for the masonry buidings which are locoated on slow-moving landslides and are perpendicular to the slope direction. The case study building is oriented along the contour lines or nearly perpendicular to the direction of the slope or the landslide. If the building was oriented parallel to slope direction, the damage would not have been so severe. It is revealed by the results obtained from the sensitivity analysis of building parameters in the assessment of vulnerability. In the case of buildings perpendicular to slope direction, the larger the building length, the more serious is the building's damage with the same force of landslide. The case study building (25 m long) showed much damage, it almost collapsed when the landslide occurred. Our study shows that the building length perpendicular to the sliding direction of the landslide should not be too large. We note that 30 m is the threshold value for the length of masonry buildings. Physical vulnerability will be decreased if the building width is increased and the length is decreased considerably (Fig 14 a and b). In this case the orientation of the building will be changed in such a way that the longest axis of the building is in the same direction of the slope. Therefore, we suggest that it is important to consider the building length-width ratio as well as the orientation of the buildings in land-use planning for the development of settlements on sloping areas.

Since the output of physical vulnerability is related to the safety factor for the area where the building is located, it is possible to evaluate the physical vulnerability of buildings prone to slow-moving landslides at a regional scale. For instance, the distribution of F_S can now be obtained from several studies (Muntohar et al 2009, Takara K et al 2010, Salciarini et al 2006 and Sorbino et al 2010). If we employ the physical vulnerability curves or the curves from this study, the risk can be quantified for the potential losses of buildings based on the *Fs* analysis for landslides at regional scale. But the application of physical vulnerability assessment at the regional scale should be tested first before implementing regional land use planning activities.

The research is based on detailed filed investigation, monitoring, and analysis in such specific landslides and case building. Concerning the limitation of this study, it is important to mention that the results are applicable for the similar geological background areas prone to slow-moving landslides or similar landslide displacement process. The quantitative relationship between the physical vulnerability of buildings and landslide displacement process is very weakly studied around the world. It needs more concentration of studies. Moreover, the physical vulnerability assessment was carried out for the building which is located inside the landslide area for which soil pressure on the foundation is suitable. Our study does not include the estimation of vulnerability for the buildings which are located acrossing the boundary of the landslide, the result of which may be a bit different. Also, we did not consider the friction between the foundation and soil, and also uncertainty analysis was not performed. In future studies, more relative mechanical models are required. Similarly, random distribution of soil parameters for landslide F_S calculation, such as shear strength, can be considered for generating fragility curves based on this study. Currently, intensive researches on slow-moving landslides vulnerability in the Three-gorges Reservoir (Zizheng G et al 2020) is strengthened, where the authors are applying our approach for more case studies. This approach will be verified and modified through continuing studies.

6 Conclusions

We propose a method for constructing physical vulnerability curves and functions by utilizing the analysis of the horizontal force of landslide acting on the foundation and the physical response of the building. The proposed method was applied to slow-moving landslides in China, for which a severely damaged building was considered as the case study structure.

The proposed method mainly comprises calculating the landslide safety factor and horizontal load on foundations based on different scenarios (extreme rainfall with different return periods); the physical response of foundation and the inclination of the building was also analyzed. Finally, the physical vulnerability curves were generated by applying the Weibull function.

Good consistency between the estimated physical vulnerability and on-field damage evidence was observed in the case study building. The sensitivity analysis of the building characteristics revealed that building length and foundation depth are the main determining factors in the physical vulnerability in the slow-moving landslides. The larger the building length, the

higher is the vulnerability. Apart from the length, the orientation of the building seems to be equally important. Thus the building length, especially if it is oriented perpendicular to the sliding direction of the landslide, should not be too large. We hope that this study can be a useful supplement for the physical vulnerability estimation of buildings in the area prone to slow-moving landslides.

Data availability. The study relied on two sets of data: (i) the data collected by the fieldwork, (ii) the detailed landslide investigation reports provided by the China Geological Survey (Hunan Institute of Xiangxi Geological Engineering Survey). The data is included in Section 3 in this paper.

Author contribution. Qin Chen and Lixia Chen discussed the research plan, carried out the fieldwork, carried out the modelling part, and wrote the paper. Qin Chen prepared the figures for the paper. Lixia Chen and Kunlong Yin supervised the research. Lei Gui and Xuelian Cao helped in modelling. Lei Gui and Juan Du helped in data collection. Shrestha helped in research paper development and English writing.

Competing interests. The authors declare that they have no conflict of interest.

Special issue statement. This article is not a part of any special issues. It is not associated with a conference.

Acknowledgments. This research is supported by two projects: (i) the project titled "Studies on spatial-temporal differences of large accumulation landslide deformation and its vulnerability model for buildings in the Three Gorges reservoir" which is financed by the National Natural Science Foundation of China [Grant No. 41877525], and (ii) the project titled "Study on the dynamic response of the quantitative vulnerability of buildings in different evolution stage of landslides" financed by the National Natural Science Foundation of China [Grant No. 41601563].

References

Abdulwahid, W. M. and Pradhan, B.: Landslide vulnerability and risk assessment for multi-hazard scenarios using airborne laser scanning data (LiDAR), Landslides, doi:10.1007/s10346-016-0744-0, 2017.

Alexander, D.: Landslide damage to buildings, Environment. Geol. Water Sci., 8(3), 147–151, 1986.

Antronico, L., Borrelli, L., Coscarelli, R., and Gullà, G.: Time evolution of landslide damages to buildings: the case study of Lungro (Calabria, southern Italy), Bull. Eng. Geol. Environ., doi:10.1007/s10064-014-0591-y, 2015.

Apip, Takara K, Yamashiki Y, et al.: A distributed hydrological-geotechnical model using satellite-derived rainfall estimates for shallow landslide prediction system at a catchment scale. Landslides 7:237–258, 2010.

Barlow, J. P.: Slope movement patterns in young valley slopes in Northern Alberta, Canada, in: Landslides in Research, Theory and Practice: Proceedings of the 8th International Symposium on Landslides held in Cardiff on 26–30 June 2000.

Borrelli, L., Nicodemo, G., Ferlisi, S., Peduto, D., Di Nocera, S., and Gullà, G.: Geology, slow-moving landslides, and damages

to buildings in the Verbicaro area (North-western Calabria region, southern Italy), J. Maps, doi:10.1080/17445647.2018.1425164, 2018.

Brooker, E. W. and Peck, R. B.: Rational design treatment of slides in overconsolidated clays and clay shales, Canadian Geotech. J., doi:10.1139/t93-045, 1993.

Burland, J. B. and Wroth, C. P.: Settlement of buildings and associated damage, in Settlement of Structures, Proc. Conf. Brit. Geotech. Soc., 1974.

Burland, J. B., Broms, B.B., and Mello, V., Behaviour of foundation and structures, Comportent des Foundations et des Structures, 1977.

Cascini, L., Calvello, M., and Grimaldi, G.: Modelling the transient groundwater regime for the displacements analysis of slow-moving active landslides, in: Landslides and Engineered Slopes, From the Past to the Future. 2008.

Chen, J., Rong, Y., Qiang, W., Jie, T., He, Z., Cao, H., Observatory, H. M., Service, C. M., Service, D. M., and Service, H. M.: Hazard rainfall threshold analysis of rainfall-induced geological disasters in Hunan Province, J. Catastroph., 2014.

Chen, L., Cao, X., Yin, K., Wu, Y., and Li, Y.: Physical vulnerability assessment for buildings impacted by a slow moving landslide based on field work and statistical modelling, in: Landslides and Engineered Slopes. Experience, Theory and Practice, 2016.

China Railway Second Survey and Design Institute: Design and calculation of anti-slide pile, 1983.

Chiocchio, C., Iovine, G., and Parise, M.: A proposal for surveying and classifying landslide damage to buildings in urban areas, Engineering geology and the environment. Proc. Sympsium, Athens, 1, 1997.

Ciurean, R. L., Hussin, H., van Westen, C. J., Jaboyedoff, M., Nicolet, P., Chen, L., Frigerio, S., and Glade, T.: Multi-scale debris flow vulnerability assessment and direct loss estimation of buildings in the Eastern Italian Alps, Natural Hazards, doi:10.1007/s11069-016-2612-6, 2017.

Ciurean, L. R., Schroter, D., and Glade, T.: Conceptual frameworks of vulnerability assessments for natural disasters reduction, in: Approaches to Disaster Management - Examining the Implications of Hazards, Emergencies and Disasters, 2013.

Clifton, A. W., Yoshida, R. T., and Chursinoff, R. W.: Regina Beach - a town on a landslide, Canadian Geotech. J., doi:10.1139/t86-007, 1986.

Cooper, A. H.: The classification, recording, databasing and use of information about building damage caused by subsidence and landslides, Quart. J. Eng. Geol. Hydrogeol., doi:10.1144/1470-9236/07-223, 2008.

Corominas, J., van Westen, C., Frattini, P., Cascini, L., Malet, J. P., Fotopoulou, S., Catani, F., Van Den Eeckhaut, M., Mavrouli, O., Agliardi, F., Pitilakis, K., Winter, M. G., Pastor, M., Ferlisi, S., Tofani, V., Hervás, J., and Smith, J. T.: Recommendations for the quantitative analysis of landslide risk, Bull. Eng. Geol. Environ., doi:10.1007/s10064-013-0538-8, 2014.

Cruden, D.M, Varnes: Landslide types and process, 1996

Cui, P., Xiang, L. Z., and Zou, Q.: Risk assessment of highways affected by debris flows in Wenchuan earthquake area, J. Mount. Sci., doi:10.1007/s11629-013-2575-y, 2013.

Dai, Z.: Study on distribution laws of landslide-Thrust and resistance of sliding mass acting on antislide piles, Chinese J. Rock Mech. Eng., 2002.

Del Soldato, M., Bianchini, S., Calcaterra, D., De Vita, P., Martire, D. Di, Tomás, R., and Casagli, N.: A new approach for landslide-induced damage assessment, Geomatics Nat. Hazards Risk, doi:10.1080/19475705.2017.1347896, 2017.

Dong, J., Liao, M., Xu, Q., Zhang, L., Tang, M., and Gong, J.: Detection and displacement characterization of landslides using multi-temporal satellite SAR interferometry: A case study of Danba County in the Dadu River Basin, Eng. Geol., doi:10.1016/j.enggeo.2018.04.015, 2018.

Douglas, J.: Physical vulnerability modelling in natural hazard risk assessment, Nat. Hazards Earth Syst. Sci., doi:10.5194/nhess-7-283-2007, 2007.

Du, J., Yin, K., Nadim, F., and Lacasse, S.: Quantitative vulnerability estimation for individual landslides, in: 18th International Conference on Soil Mechanics and Geotechnical Engineering: Challenges and Innovations in Geotechnics, ICSMGE

2013, 2013.

Esser, A.J.: Case of a slope failure in lacustrine deposits, in: Landslides in Research, Theory and Practice: Proceedings of the 8th International Symposium on Landslides held in Cardiff on 26–30 June, 2000.

Faella, C. and Nigro, E.: Dynamic impact of the debris flows on the constructions during the hydrogeological disaster in Campania-1998: failure mechanical models and evaluation of the impact velocity, in: Proceedings of the International Conference on “Fast Slope Movements-Prediction and Prevention for Risk Mitigation” May,2003 Patron Editore, Napoli (pp. 179-186).

Fell, R., Corominas, J., Bonnard, C., Cascini, L., Leroi, E., and Savage, W. Z.: Guidelines for landslide susceptibility, hazard and risk zoning for land-use planning, Eng. Geol., doi:10.1016/j.enggeo.2008.03.014, 2008.

FEMA:HAZUS-MH, Technical manual, Federal Emergency Management agency, Washington DC, 2003.

Ferlisi, S., Gullà, G., Nicodemo, G., and Peduto, D.: A multi-scale methodological approach for slow-moving landslide risk mitigation in urban areas, southern Italy, Euro-Mediterranean J. Environ. Integr., doi:10.1007/s41207-019-0110-4, 2019.

Ferlisi, S., Peduto, D., Gullà, G., Nicodemo, G., Borrelli, L., and Fornaro, G.: The use of DInSAR data for the analysis of building damage induced by slow-moving landslides, 2015.

Finno, R. J., Voss, F. T., Rossow, E., and Blackburn, J. T.: Evaluating damage potential in buildings affected by excavations, J. Geotech. Geoenviron. Eng., doi:10.1061/(asce)1090-0241(2005)131:10(1199), 2005.

General Administration of Quality Supervision, Inspection and Quarantine of the PRC: Code for geological investigation of landslide prevention,2016.

Godfrey, A., Ciurean, R. L., van Westen, C. J., Kingma, N. C., and Glade, T.: Assessing vulnerability of buildings to hydro-meteorological hazards using an expert based approach - An application in Nehoiu Valley, Romania, Int. J. Disaster Risk Reduct., doi:10.1016/j.ijdrr.2015.06.001, 2015.

Guillard-Goncalves, C., Zezere, J. L., Pereira, S., and Garcia, R. A. C.: Assessment of physical vulnerability of buildings and analysis of landslide risk at the municipal scale: Application to the Loures municipality, Portugal, Nat. Hazards Earth Syst. Sci., doi:10.5194/nhess-16-311-2016, 2016.

Huang, L., Xiao, Z., Nie, W., Shi, Y., and Yang, J.: Assessment of building impacted by tunnel construction based on the statistical analysis, Chinese J. Underground Space Eng., 11(5), 1310–1315, 2015.

Huang, W., Fang, Q., Wang, G. W., and Ming-Bo, L. I.: Preliminary study on the critical rainfall for landslide space early warning in chaling county of Hunan province, Chinese J. Geol. Hazard Cont., 2014.

Infante, D., Confuorto, P., Di Martire, D., Ramondini, M., and Calcaterra, D.: Use of DInSAR data for multi-level vulnerability assessment of urban settings affected by slow-moving and intermittent landslides, in: Procedia Engineering, 2016.

James M. G., Stephen P. T.: Mechanics of Materials, 1984.

Jworchan, I., O.Ä ôBrien, A., and Rizakalla, E.: Landslide stabilization for residential development, in: Landslides and Engineered Slopes. From the Past to the Future, 2008.

Kang, H., Kim, Y.: The physical vulnerability of different types of building structure to debris flow events. Natural Hazards 80, 1475–1493 (2016). https://doi.org/10.1007/s11069-015-2032-z,2016

King, A. and Bell, R.: RiskScape New Zealand: A multihazard loss modelling tool, in: Proceedings of Earthquake Engineering in the 21st Century (EE-21C) conference, topic (Vol. 8), 2005.

King, A., and Bell, R.: RiskScape New Zealand: A multihazard loss modelling tool, in: Proceedings of Earthquake Engineering in the 21st Century (EE-21C) conference, topic (Vol. 8), 2005.

Lei, G. J., Yin, J. X., Wang, W. C., and Wang, H.: The analysis and improvement of the fuzzy weighted optimum curve-fitting method of Pearson – Type III Distribution, Water Res. Manag., doi:10.1007/s11269-018-2055-9, 2018.

Li, Z., Nadim, F., Huang, H., Uzielli, M., and Lacasse, S.: Quantitative vulnerability estimation for scenario-based landslide hazards, Landslides, doi:10.1007/s10346-009-0190-3, 2010.

Liang, Y. and Xiong, F.: Quantification of debris flow vulnerability of typical bridge substructure based on impact force simulation, Geomatics Nat. Hazards Risk, doi:10.1080/19475705.2019.1641564, 2019.

Luna, B. Q., Blahut, J., Camera, C., Westen, C. Van, Apuani, T., Jetten, V., and Sterlacchini, S.: Physically based dynamic run-out modelling for quantitative debris flow risk assessment: a case study in Tresenda, northern Italy, Environ. Earth Sci., 72(3), 645–661, 2014.

Mansour, M. F., Morgenstern, N. R., and Martin, C. D.: Expected damage from displacement of slow-moving slides, Landslides, doi:10.1007/s10346-010-0227-7, 2011.

Mavrouli, O., Giannopoulos, P. G., Carbonell, J. M., and Syrmakezis, C.: Damage analysis of masonry structures subjected to rockfalls, Landslides, 14(3), 891–904, 2017.

Ministry of Construction of the PRC: Code of Deformation Measurement of Building and Structure , 2007.

Ministry of Housing and Urban–Rural Development of PRC: Standard for dangerous building appraisal, 2016.

Ministry of Housing and Urban–Rural Development of PRC: Techinical code for building slope engineering, 2013.

Ministry of Housing and Urban–Rural Development of PRC: Technical Specification for Incline-rectifying of Buildings, 2012.

Ministry of Land and Resources of the PRC: Specification of Risk Assessment for Geological Hazard,2015.

Moore, D. P., Watson, A. D., and Martin, C. D.: September. Deformation mechanism of a large rockslide inundated by a reservoir, in: Proceedings of JTC Workshop on the Mechanics and Velocity of Large Landslides, Courmayeur, Italy, 2006.

Muntohar AS, Liao HJ.: Analysis of rainfall-induced infinite slope failure during typhoon using a hydrological-geotechnical model. Environ Geol 56:1145–1159, 2009.

Negulescu, C. and Foerster, E.: Parametric studies and quantitative assessment of the vulnerability of a RC frame building exposed to differential settlements, Nat. Hazards Earth Syst. Sci., 10(9), 1781–1792, 2010.

Nicodemo, G., Ferlisi, S., Peduto, D., Aceto, L., and Gullà, G.: Damage to masonry buildings interacting with slow-moving landslides: A numerical analysis, in: Lecture Notes in Civil Engineering, 2020.

Nicodemo, G., Peduto, D., Ferlisi, S., Gullà, G., Borrelli, L., Fornaro, G., and Reale, D.: Analysis of building vulnerability to slow-moving landslides via A-DInSAR and damage survey data, in: Advancing Culture of Living with Landslides, 2017.

Nie, W. N., Zhang, L., and Hu J., 2004. Study on designed thrust of anti-slide pile. Chinese J. Rock Mech. Eng., 23(5), 050-5.

Papathoma-Köhle, M., Zischg, A., Fuchs, S., Glade, T., and Keiler, M.: Loss estimation for landslides in mountain areas - An integrated toolbox for vulnerability assessment and damage documentation, Environ. Model. Software, doi:10.1016/j.envsoft.2014.10.003, 2015.

Peduto, D., Ferlisi, S., Nicodemo, G., Reale, D., Pisciotta, G., and Gullà, G.: Empirical fragility and vulnerability curves for buildings exposed to slow-moving landslides at medium and large scales, Landslides, doi:10.1007/s10346-017-0826-7, 2017.

Peduto, D., Nicodemo, G., Caraffa, M., and Gullà, G.: Quantitative analysis of consequences to masonry buildings interacting with slow-moving landslide mechanisms: a case study, Landslides, doi:10.1007/s10346-018-1014-0, 2018.

Peng, L., Xu, S., Hou, J., and Peng, J.: Quantitative risk analysis for landslides: the case of the Three Gorges area, China, Landslides, doi:10.1007/s10346-014-0518-5, 2015.

Qiong, F., Quanming, C., and Langhui, W. U.: Analysis of rainstorm-induced geological disasters in Hunan Province and its enlightenment for disaster prevention, J. Inst. Disast. Prevent., 2018.

Radwan, F., Alazba, A. A., and Mossad, A.: Flood risk assessment and mapping using AHP in arid and semiarid regions, Acta Geophysica, doi:10.1007/s11600-018-0233-z, 2019.

Salciarini, D., Godt, J. W., Savage, W. Z., Conversini, P., Baum, R. L. and Michael, J. A.: Modeling regional initiation of rainfall-induced shallow landslides in the eastern Umbria Region of central Italy, Landslides, doi:10.1007/s10346-006-0037-0, 2006.

Sedan, O., Negulescu, C., Terrier, M., Roulle, A., Winter, T., and Bertil, D.: Armagedom - A tool for seismic risk assessment illustrated with applications, J. Earthquake Eng., doi:10.1080/13632469.2012.726604, 2013.

Sedan, O., Negulescu, C., Terrier, M., Roullé, A., Winter, T., and Bertil, D., 2013. Armagedom—a tool for seismic risk assessment illustrated with applications, J. Earthquake Eng., 17(2), 253–281.

Singh, V. P. and Singh, K.: Parameter estimation for Log-pearson type III distribution by POME, J. Hydraulic Eng.,

doi:10.1061/(asce)0733-9429(1988)114:1(112), 1988.

Sorbino, G., Sica, C. and Cascini, L.: Susceptibility analysis of shallow landslides source areas using physically based models, Natural Hazards, doi:10.1007/s11069-0, 2010.

Sterlacchini, S., Frigerio, S., Giacomelli, P., and Brambilla, M.: Landslide risk analysis: A multi-disciplinary methodological approach, Nat. Hazards Earth Syst. Sci., doi:10.5194/nhess-7-657-2007, 2007.

Tarbotton, C., Dall'osso, F., Dominey-Howes, D., Goff, J. The use of empirical vulnerability functions to assess the response of buildings to tsunami impact: comparative review and summary of best practice. Earth Sci. Rev. 142, 120–134, doi.org/10.1016/j.earscirev.2015.01.002, 2015.

Totschnig, R., Sedlacek, W., and Fuchs, S., 2011. A quantitative vulnerability function for fluvial sediment transport. Nat. Hazards, 58(2), 681–703.

UNDRO: Disaster prevention and mitigation : a compendium of current knowledge / Office of the United Nations Disaster Relief Co-ordinator, United Nations, Geneva., 1986.

Uzielli, M., Catani, F., Tofani, V., and Casagli, N.: Risk analysis for the Ancona landslide—I: characterization of landslide kinematics, Landslides, doi:10.1007/s10346-014-0474-0, 2015a.

Uzielli, M., Catani, F., Tofani, V., and Casagli, N.: Risk analysis for the Ancona landslide—II: estimation of risk to buildings, Landslides, doi:10.1007/s10346-014-0477-x, 2015b.

van Westen, C. J., van Asch, T. W. J., and Soeters, R.: Landslide hazard and risk zonation - Why is it still so difficult?, Bull. Eng. Geol. Environ., doi:10.1007/s10064-005-0023-0, 2006.

Varnes, D.: Landslide hazard zonation: a review of principles and practice, Nat. Hazards, (3), 1984.

Wang, S., Wu, W., Wang, J., Yin, Z., Cui, D., and Xiang, W.: Residual-state creep of clastic soil in a reactivated slow-moving landslide in the Three Gorges Reservoir Region, China, Landslides, doi:10.1007/s10346-018-1043-8, 2018.

Wasowski, J., Casarano, D., Bovenga, F., Refice, A., Nutricato, R., and Nitti, D.O.: Landslide-prone towns in Daunia (Italy): PS interferometry-based investigation, in: Landslides and Engineered Slopes, From the Past to the Future, 2008.

Weibull, W., 1951. A statistical distribution function of wide applicability. J. Appl. Mech., 18(3), 293–297.

Winter, M. G., Smith, J. T., Fotopoulou, S., Pitilakis, K., Mavrouli, O., Corominas, J., and Argyroudis, S.: An expert judgement approach to determining the physical vulnerability of roads to debris flow, Bull. Eng. Geol. Environ., doi:10.1007/s10064-014-0570-3, 2014.

Yue, W. U., Liu, D. S., Xin, L. U., and Song, Q. H.: Vulnerability assessment model for hazard bearing body and landslide risk index, Rock Soil Mech., 32(8), 1009–2487, 2011.

Zhang, Y., Meng, X., Jordan, C., Novellino, A., Dijkstra, T., and Chen, G.: Investigating slow-moving landslides in the Zhouqu region of China using InSAR time series, Landslides, doi:10.1007/s10346-018-0954-8, 2018.

Zizheng Guo, Lixia Chen, Kunlong Yin, Dhruba Pikha Shrestha, Liang Zhang. Quantitative risk assessment of slow-moving landslides from the viewpoint of decision-making: A case study of the Three Gorges Reservoir. Engineering Geology .2020 .DOI: https://doi.org/10.1016/j.enggeo.2020.

Zou, Q., Cui, P., Zhou, G. G. D., Li, S., Tang, J., and Li, S.: A new approach to assessing vulnerability of mountain highways subject to debris flows in China, Progress Phys. Geo., doi:10.1177/0309133318770985, 2018.